Localized Bose-Einstein condensation in disordered liquid ^{4}He films

Jacques Bossy,[1] Helmut Schober,[2,3] and H. R. Glyde[4]
[1]*Institut Néel, CNRS-UJF, BP 166, 38042 Grenoble Cedex 9, France*
[2]*Institut Laue-Langevin, BP 156, 38042 Grenoble, France*
[3]*Université Joseph Fourier, UFR de Physique, F38041 Grenoble Cedex 9, France*
[4]*Department of Physics and Astronomy, University of Delaware, Newark, Delaware 19716-2593, USA*
(Received 23 October 2014; published 3 March 2015)

We present neutron scattering measurements of the phonon-roton and layer modes of liquid helium films adsorbed in 25-Å pore diameter gelsil as a function of temperature. The goal is to determine whether the well-defined phonon-roton and layer modes observed at low temperature at partial fillings of the porous media persist as well-defined modes at higher temperatures above the superfluid phase, as is the case of fully filled pores (3D liquid). We find that well defined P-R modes exist in films at temperatures well above the superfluid phase. This is the case at all fillings investigated. Liquid ^{4}He in porous media is an example of a Bose liquid in disorder. The existence of P-R modes above T_c suggests the existence of patches or islands of Bose condensed liquid that have order [localized Bose-Einstein condensation (LBEC)] above T_c. The interpretation is that the well-defined P-R modes propagate in the patches of BEC. Gelsil partially filled with liquid helium shows the same LBEC behavior as found previously in fully filled gelsil (as in a 3D liquid).

DOI: 10.1103/PhysRevB.91.094201 PACS number(s): 67.25.dt, 67.25.dr, 67.10.Ba, 61.05.fg

I. INTRODUCTION

Liquid ^{4}He confined in porous media is an example of Bosons in disorder. It is also a Bose liquid confined to nanoscales. The superfluid density, ρ_S, and the critical temperature, T_c, for superflow of this dense Bose liquid have been extensively investigated in several porous media [1–3]; in aerogels, Vycor, Xerogel, gelsils [4], and FSM [5–9], for example. The confinement to nanoscales and the disorder reduces T_c below the bulk value, T_λ. The smaller the pore diameter, the further T_c is reduced below T_λ. For example, at saturated vapor pressure (SVP) where $T_\lambda = 2.17$ K, $T_c =$ 1.95–2.05 K in 70-Å mean pore diameter (MPD) Vycor [10–12] and 0.7–1.4 K in 25-Å MPD gelsil [4,13].

The temperature dependence of ρ_S below T_c also differs from that in the bulk. For example, in porous media, the critical exponent γ, governing the superfluid density immediately below T_c, $\rho_S/\rho = (1 - T/T_c)^\gamma$, generally differs [2,10,14] from the bulk value $\gamma = 0.67$. At intermediate temperature, the $\rho_S(T)/\rho$ is well described by the Landau theory in terms of excitation of the layer modes that exist in porous media [15,16] rather than the phonon-roton mode as in the bulk. Recent interest has moved to smaller pore media and to measurements [4,7,8,13] of ρ_S under pressure to determine the superfluid phase diagram and ρ_S as a function of pressure and temperature.

The excitations of liquid ^{4}He in several media have been investigated. Observed is the phonon roton (P-R) mode, as in bulk liquid ^{4}He, and a layer mode, a density mode (or modes) that propogates in the liquid adjacent to the porous media walls. Specifically, the layer mode propagates in the 2–5 liquid layers that lie on the amorphous solid layers of ^{4}He on the walls. The goal is to characterize these modes and relate them to the superfluid and thermodynamic properties of liquid ^{4}He. In fully filled porous media at SVP, the P-R mode energy is the same as in the bulk liquid within precision, both at low T and as a function of T in all porous media investigated [12,17–22]. To date, the layer mode is observed [12,17,18,20–27] at wave vectors $1.7\ \text{Å}^{-1} < Q < 2.3\ \text{Å}^{-1}$ only, denoted the roton region. At these wave vectors, the layer mode energy, ω_L, has a rotonlike dispersion with an energy minimum near $Q = 2.1\ \text{Å}^{-1}$. At this minimum, the mode is denoted the "layer roton" and has an energy Δ_L that lies 0.2–0.3 meV below the bulk roton minimum, $\Delta = 0.742 \pm 0.001$ meV. For this reason, the superfluid density at intermediate temperatures [15] and the specific heat [21,28] in porous media are governed by exciting the lower energy layer mode (rather than the P-R mode).

In bulk liquid ^{4}He, well-defined P-R modes at higher wave vectors ($Q \lesssim 0.7\ \text{Å}^{-1}$) exist only in the superfluid phase [29–33] where there is Bose-Einstein condensation [34] (BEC). In contrast, in porous media, well-defined modes are observed at temperatures above the superfluid phase [12,16,20,26]. For example, at SVP in Vycor [12,16] and in 25-Å and 44-Å MPD gelsil [20,26], well-defined modes were observed at temperatures above T_c and up to close to T_λ. The temperature at which P-R modes are last observed is denoted $T_{\rm PR}$. Since well-defined P-R modes at higher wave vectors are expected to exist only where there is BEC, this suggests that $T_{\rm PR}$ coincides with $T_{\rm BEC}$, the onset temperature of BEC. Indeed, there are sound theoretical arguments [35–39] going back to Bogoliubov [35] that sharply-defined P-R modes are expected when there is BEC, but not otherwise. This suggests that there is BEC at temperatures above T_c in porous media, up to $T_{\rm BEC} = T_{\rm PR} \simeq T_\lambda$.

Under pressure, T_c is further reduced [4,19] and, remarkably, T_c is observed to go to zero at $p = 34$ bar in 25-Å MPD gelsil [4]. This suggests a quantum phase transition (QPT) from the superfluid to the normal liquid phase at $p = 34$ bar [4]. In contrast, at 34 bar, well-defined P-R modes are observed up to $T_{\rm PR} = 1.5$ K, e.g., $T_{\rm BEC} \simeq 1.5$ K, in 25-, 34-, and 44-Å gelsil [19,27,40] and in 47-Å MCM-41 [21,27]. In 28-Å FSM, Taniguchi *et al.* [8] show that T_c decreases rapidly with increasing pressure indicating that T_c will go to zero at approximately 20 bar before the liquid solidifies. $T_{\rm BEC} = T_{\rm PR}$

 ©2015 American Physical Society

apparently lies well above T_c so that T_{BEC} is much less sensitive to pore size and structure than is T_c.

The temperature range $T_c < T < T_{BEC}$ is interpreted as a region in which there is BEC localized (LBEC) to patches or islands separated by a normal liquid [12,16,20,26,28]. The phase of the BEC in each island is independent and unconnected so that there is no continuous, connected phase coherence across the sample as needed for superflow. However, the islands are large enough (e.g., 15–20-Å diameter) to support well-defined P-R modes that are observed by neutrons.

Superfluidity in films on surfaces and on the walls of porous media has similarly been extensively investigated [41–48]. At low temperature, a threshold coverage is needed before superfluidity is observed. In a wide variety of media, the threshold coverage [48] is $n_0 = 26\ \mu\text{mol/m}^2$. The interpretation is that up to the threshold n_0, the helium is deposited in inert layers on the media walls. These are amorphous solid and bound liquid layers with boson localization induced by the rough media walls. For higher coverages $n > n_0$, the additional helium is deposited as liquid that supports superflow. Also for $n > n_0$, T_c increases linearly with coverage with T_c proportional to $n - n_0$. At low values of $n - n_0$, there is a small deviation from linearity seen universally on all surfaces [48] that suggests universal "boson localization" in the inert layers. Eventually, at full filling, T_c reaches the 3D values discussed above.

The goal of this paper is to present parallel measurements of the P-R modes at partial fillings. The temperature dependence of P-R modes in films has not as yet been reported. Particularly, we seek the highest temperature T_{PR} at which the P-R mode is observed. Taking T_{PR} as the onset temperature of BEC, we can compare $T_{BEC} = T_{PR}$ with T_c and determine whether there is a LBEC phase at partial fillings (in reduced dimension) as there is at full filling. We can also compare the threshold filling for superflow, n_0, with the filling at which P-R are first observed. We choose the porous medium 25-Å MPD gelsil because the superfluid phase and T_c have been measured [4] as a function of filling from $n = 0$ to full filling and because T_c lies well below T_λ.

II. EXPERIMENT

A. Gelsil porous medium

The 25-Å mean pore diameter (MPD) gelsil was kindly provided by Keiya Shirahama. It is from the same batch of gelsil as used in his group's measurements of the superfluid density, the specific heat, and the phase diagram of helium in 25-Å gelsil [4,49,50] and as used by us in previous measurements [27,40]. It was fabricated by 4F International Co. using a sol-gel technique and characterized by them using N_2 adsorption-desorption isotherms at 76 K. The isotherms were analyzed using the standard Barrett, Joyner, and Halenda (BJH) model [51], which indicated the MPD quoted with a broad, approximately Gaussian distribution of pore diameters of half width at half maximum of 20 Å (see Ref. [40]). The gelsil had a pore volume of $0.376\,\text{cm}^3/\text{g}$ and surface area of $586\,\text{m}^2/\text{g}$ as determined similarly by 4F International from N_2 isotherms. Prior to the neutron scattering measurements, the sample was cleaned by heating it at 100 °C under vacuum for 10 hours as done in previous measurements [26,27].

B. Neutron scattering experiment

The gelsil sample consisted of two monolithic cylinders, one of diameter 8.76 mm and height 17.64 mm and the other of diameter 8.85 mm and height 17.79 mm. The two cylinders had a total mass of 2.93 g and volume of $2.16\,\text{cm}^3$. With a pore volume of $0.376\,\text{cm}^3/\text{g}$, the sample had a total pore volume of $1.11\,\text{cm}^3$ (a porosity of 51%).

The two cylinders were placed one on top of the other in the cylindrical Al sample cell as shown in Fig. 2 of Ref. [40]. The internal diameter of the sample cell was 10.2 mm. The top and bottom of the cell, above and below the cylinders, respectively, was shielded from the neutron beam by Cd rings. The cell was cooled with a ^{3}He fridge. Helium in the gelsil condenses first as inert layers on the pore walls. Liquid that supports modes begins to condense at a filling of approximately 73% in 25-Å MPD gelsil [26].

The neutron scattering experiment was performed on the time of flight spectrometer IN6 at the Institut Laue-Langevin, Grenoble, France. An incident neutron wavelength of 4.14 Å was used, which provided a spectrometer energy resolution of 0.16 meV at the elastic line ($\omega = 0$).

C. Adsorption isotherm

Prior to the neutron experiment, a helium adsorption isotherm measurement was conducted. All the experimental conditions of the isotherm were the same as those for the neutron experiment. The same filling capillary, sample cell, and pressure gauge were used. The isotherm, which was conducted at $T = 1.90$ K, is shown in Fig. 1. At $T = 1.90$ K the saturated vapor pressure (SVP) of bulk liquid ^{4}He is $P_{Sat} = 24.3$ mbars.

D. The model $S(Q,\omega)$

To analyze the data and identify the P-R and layer (L) modes, particularly their dependence on filling and temperature, we require a model of the dynamical structure factor

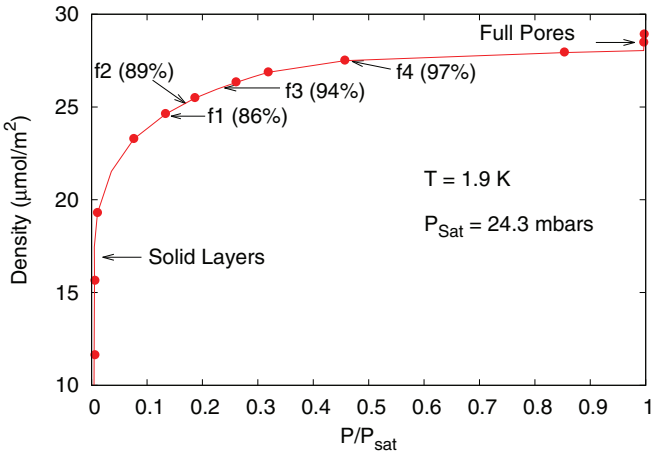

FIG. 1. (Color online) Absorption isotherm of helium in the present 25-Å mean pore diameter (MPD) gelsil. Shown is the amount of ^{4}He adsorbed vs the vapor pressure P of helium above the gelsil. P_{Sat} is the saturated vapor pressure of bulk helium at 1.9 K. When $P = P_{Sat}$, the gelsil is full and bulk liquid can form.

(DSF), $S(Q,\omega)$. The present model consists of a P-R mode, a layer (L) mode and a normal liquid (N) component. The model was fitted to the net scattering intensity from the ^{4}He in the porous media. The weights in each component are determined by fits to data as a function of filling and temperature.

To begin, we measured the scattering intensity at a filling of 28% at $T = 0.4$ K. This was taken as a background $S_B(Q,\omega)$ arising from scattering from the inert layers of ^{4}He on the gelsil walls at this specific filling. In $S(Q,\omega)$ at higher fillings, we also included an additional broad component, $S_A(Q,\omega)$, which arises from scattering from additional inert layers as filling is increased. It may also include some multiple scattering at higher fillings. The additional intensity, $S_A(Q,\omega)$ is small and completely negligible compared to the P-R mode at $Q \simeq 2$ Å (see Fig. 7). In addition, $S_A(Q,\omega)$ contributes at higher energy, at energies above the P-R mode. At lower Q where $S_A(Q,\omega)$ is not negligible, it can be readily separated from the P-R mode.

Specifically, we write the DSF as

$$S(Q,\omega) = S_{\rm PR}(Q,\omega) + S_L(Q,\omega) + S_N(Q,\omega) + [S_B(Q,\omega) + S_A(Q,\omega)], \quad (1)$$

$S_{\rm PR}(Q,\omega)$, $S_L(Q,\omega)$, and $S_N(Q,\omega)$ are the P-R mode, the layer mode, and the normal liquid components, respectively. $S_B(Q,\omega)$ is independent of filling and temperature. $S_A(Q,\omega)$ increases somewhat with filling but is held independent of temperature. $S_{\rm PR}(Q,\omega)$, $S_L(Q,\omega)$, and $S_N(Q,\omega)$ are determined from fits to the remaining net $S(Q,\omega)$.

1. The dynamic structure factors

The P-R mode DSF is represented by a damped harmonic oscillator (DHO) function,

$$S_{\rm PR}(Q,\omega) = (1/2\pi)[n_B(\omega)+1]A_D(Z_Q,\omega_Q,\Gamma_Q), \quad (2)$$

where $n_B(\omega) = [\exp(\hbar\omega/k_BT)-1]^{-1}$ is the Bose function and $A_D(Q,\omega)$ is the DHO spectral function [30,52,53]

$$A_D(Z_Q,\omega_Q,\Gamma_Q) = Z_Q\left[\frac{2\Gamma_Q}{(\omega-\omega_Q)^2+\Gamma_Q^2} - \frac{2\Gamma_Q}{(\omega+\omega_Q)^2+\Gamma_Q^2}\right], = Z_Q\left\{\frac{8\omega\omega_Q\Gamma_Q}{\left(\omega^2-\left[\omega_Q^2+\Gamma_Q^2\right]\right)^2+4\omega^2\Gamma_Q^2}\right\}. \quad (3)$$

The corresponding imaginary part of the dynamical susceptibility is $\chi_D''(Q,\omega) = -2A_D(Q,\omega)$. The fitting parameters are ω_Q, Γ_Q, and Z_Q, the P-R mode frequency, half-width, and intensity, respectively.

The normal liquid DSF is also represented by a DHO function,

$$S_N(Q,\omega) = (1/2\pi)[n_B(\omega)+1]A_D(Z_N,\omega_N,\Gamma_N), \quad (4)$$

with Z_N, ω_N, and Γ_N as fitting parameters. Since $S_N(Q,\omega)$ is a broad function, the Γ_N and ω_N have no meaning as a mode energy and half width. The DHO is simply a convenient function that provides a good fit to the data at high temperature.

The layer mode $S_L(Q,\omega)$ is represented by a Gaussian (G) function,

$$S_L(Q,\omega) = [n_B(\omega)+1]A_G(Z_L,\omega_L,\sigma_L), \quad (5)$$

$$A_G(Z_L,\omega_L,\sigma) = Z_L\left[\frac{1}{\left(2\pi\sigma_L^2\right)^{1/2}}\right]\exp-\frac{(\omega-\omega_L)^2}{2\sigma_L^2}. \quad (6)$$

In $S_L(Q,\omega)$, the fitting parameters are Z_L, ω_L, and σ_L. The mode width (FWHM) is related to σ_L by $2\Gamma_L = 2\sigma_L(2\ln 2)^{1/2}$ or $\sigma_L = (2\Gamma_L)/2(2\ln 2)^{1/2}$. The layer mode may be a single mode or a sum of modes and ω_L, and $2\Gamma_L$ represent the center of intensity and the width of the mode or modes, respectively.

2. Low temperature

At low temperature where there is little or no normal liquid, we assume $S_N(Q,\omega) = 0$. The model then reduces to

$$S(Q,\omega) = S_{\rm PR}(Q,\omega) + S_L(Q,\omega) + [S_B(Q,\omega) + S_A(Q,\omega)]. \quad (7)$$

Given $S_B(Q,\omega)$, the parameters in $S_{\rm PR}(Q,\omega)$ and $S_L(Q,\omega)$ and the function $S_A(Q,\omega)$ are determined by fits to the net data at the lowest temperature, $T = 0.4$ K.

3. High temperature

As temperature is increased, the intensity in $S_{\rm PR}(Q,\omega)$ and $S_L(Q,\omega)$ decreases. At the highest temperature (e.g., $T = 2.2$ K), $S_{\rm PR}(Q,\omega)$ and $S_L(Q,\omega)$ are negligible and the model reduces to

$$S(Q,\omega) = S_N(Q,\omega) + [S_B(Q,\omega) + S_A(Q,\omega)]. \quad (8)$$

$S_B(Q,\omega)$ and $S_A(Q,\omega)$ are held independent of temperature. The parameters in $S_N(Q,\omega)$ were initially determined by fits to the highest-temperature data where $S_N(Q,\omega)$ is dominant and the parameters in $S_N(Q,\omega)$ can be well determined. These parameters were then used as a guide but only a guide to fits at lower temperature where $S_N(Q,\omega)$ is smaller.

4. Intermediate temperature

At intermediate temperature, the full model (1) is used. As temperature increases, the weights Z_Q and Z_L in $S_{\rm PR}(Q,\omega)$ and $S_L(Q,\omega)$ decrease and that in $S_N(Q,\omega)$ increases. As a first approximation, the energy and width parameters in $S_{\rm PR}(Q,\omega)$, $S_L(Q,\omega)$, and $S_N(Q,\omega)$ were assumed to be independent of temperature and only the weights in the modes adjusted to obtain a fit at intermediate temperatures. Subsequently, the energy and width parameters were adjusted to obtain the final fits.

5. The static structure factor S(Q)

The $S(Q)$ corresponding to each component of $S(Q,\omega)$ is

$$S_{\rm PR}(Q) = \int_{-\infty}^{\infty} d\omega S_{\rm PR}(Q,\omega), \quad (9)$$

$$S_N(Q) = \int_{-\infty}^{\infty} d\omega S_N(Q,\omega), \quad (10)$$

$$S_L(Q) = \int_{-\infty}^{\infty} d\omega S_L(Q,\omega). \quad (11)$$

The total $S(Q)$ is

$$S(Q) = S_{PR}(Q) + S_L(Q) + S_N(Q). \quad (12)$$

At low temperature where $2\Gamma_Q$ is small and $\hbar\omega_Q/k_BT \ll 1$, the static structure factor for the P-R mode given by Eqs. (2) and (3) is well approximated by

$$S_{PR}(Q) = Z_Q\left[\frac{2}{\pi}\tan^{-1}\left(\frac{\omega_Q}{\Gamma_Q}\right)\right]. \quad (13)$$

In the limit $\Gamma_Q \to 0$, $S_{PR}(Q) = Z_Q$. The $S(Q)$ were used as the measure of intensity in the modes.

III. RESULTS

A. Observed data

Figure 2 shows the net scattering intensity $S(Q,\omega)$ at four fillings of gelsil versus wave vector Q and energy ω transfer. There is strong elastic scattering ($\omega = 0$) at $Q = 2$ Å^{-1} at all four fillings. This is presumably from the amorphous solid layers in the films, the layers that are bound to the gelsil walls.

Plantevin *et al.* [26] have shown that inelastic scattering from the P-R and layer modes of liquid ^{4}He in gelsil is first observed at a filling of about 73%. At higher fillings, the intensity in the modes increases approximately linearly with filling [26]. In Fig. 2, the fillings are 86% (1) to 97% (4). At filling 1, the inelastic intensity at $\omega > 0$ is highest at $Q \simeq$ 2.0–2.5 Å^{-1}. For a P-R mode that is reasonably well defined in ω and centered at an energy ω_Q, we expect an inelastic scattering intensity proportional to $(\hbar Q^2/2m)/\omega_Q$, from the f-sum rule. This Q dependence is largely observed in Fig. 2. The intensity clearly increases with increasing filling. At filling 1, the P-R mode energy, ω_Q, at $Q \simeq 1.1$ Å^{-1} (the maxon region) lies well below the bulk value given by the black line. At partial fillings and in films on surfaces, an ω_Q in the maxon region that lies below the bulk value is universally observed. As filling increases, the ω_Q moves toward the bulk value as seen at filling 4. At full filling, the P-R mode energy at all Q in all porous media investigated to date is the same as the bulk value at saturated vapor pressure (SVP).

In Fig. 2 at wave vectors $Q \simeq 1.9$ Å^{-1}, i.e., the roton region, there is significant inelastic intensity at low energies below the P-R mode as well as in the P-R mode. This is scattering intensity from the layer mode (or modes). The layer mode is observed at wave vectors in the roton region only. The P-R and

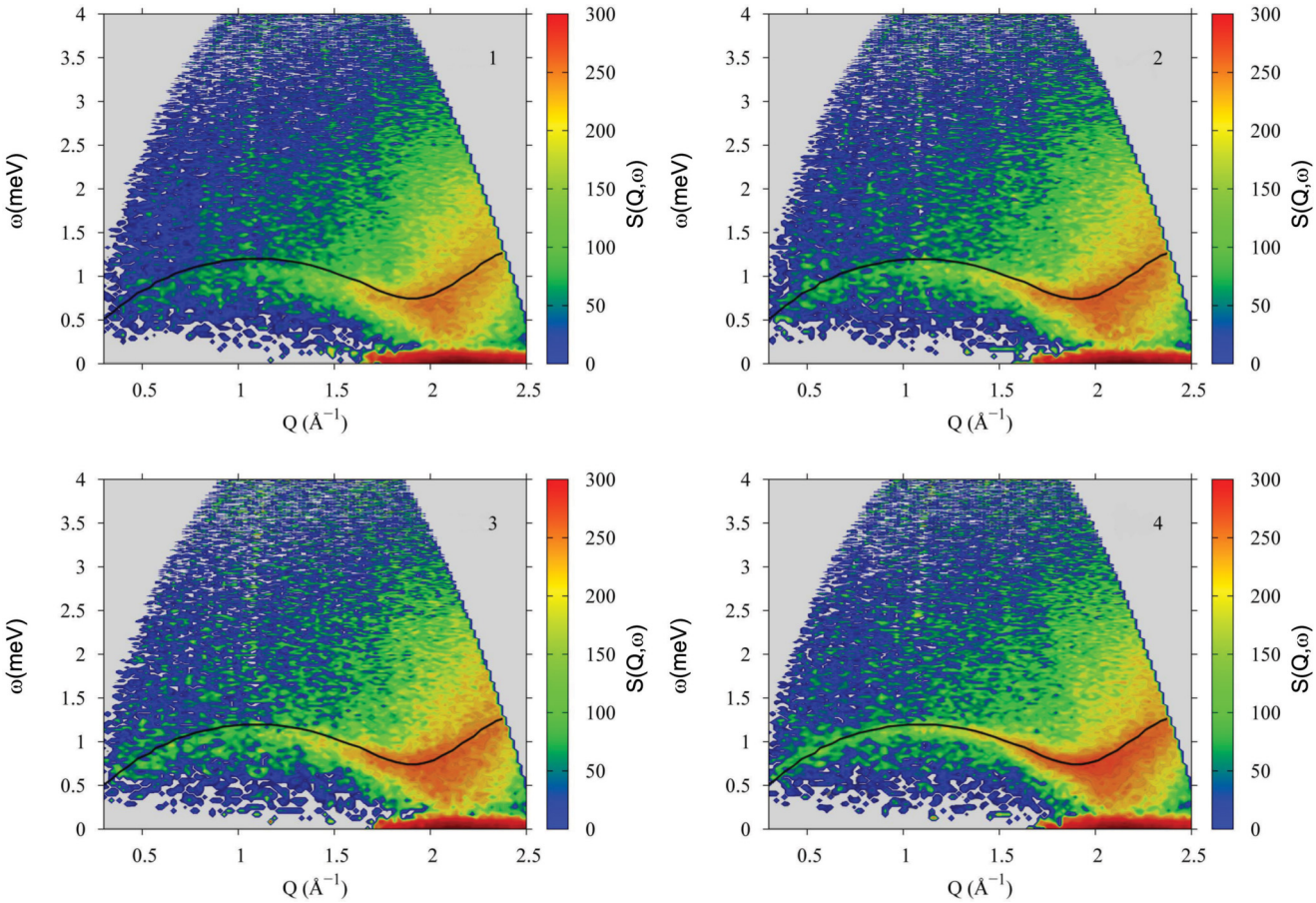

FIG. 2. (Color online) The dynamical structure factor (DSF), $S(Q,\omega)$, of liquid ^{4}He in 25-Å MPD gelsil as a function of filling. The fillings are 1 = 86% full, 2 = 89%, 3 = 91%, and 4 = 97% full. The solid black line is the phonon-roton (P-R) mode energy in bulk liquid ^{4}He at saturated vapor pressure (SVP). A P-R mode is observed at filling 1 with energy that lies below the bulk value in the maxon region $Q \simeq 1.1$ Å^{-1}. The P-R mode energy moves to the bulk value as filling increases. Intensity in $S(Q,\omega)$ at higher wave vectors, $1.5 < Q < 2.4$ Å^{-1}, and low energy, ω, is also observed, which arises from modes propagating in the liquid adjacent to the pore walls, denoted layer modes.

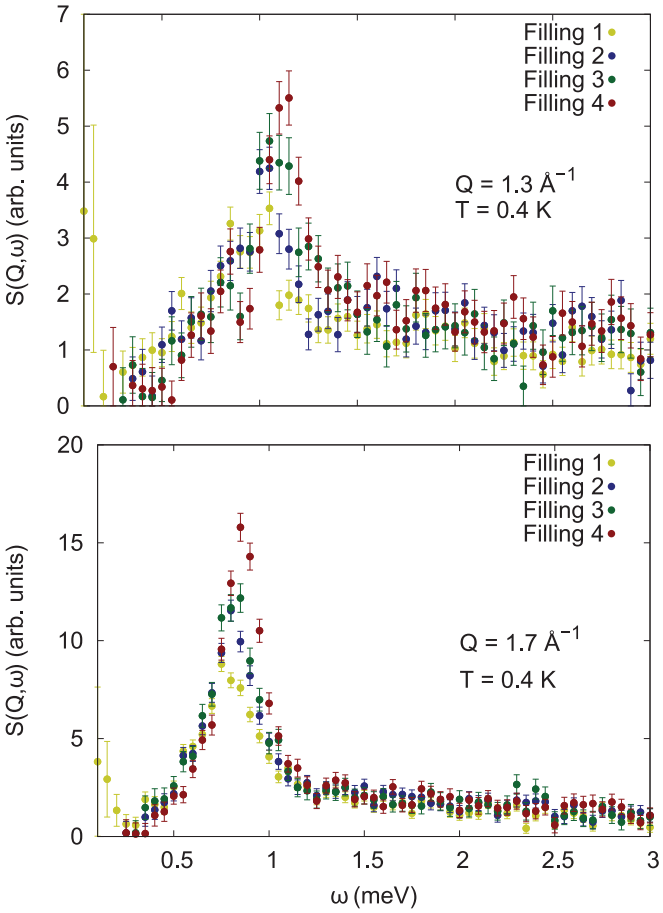

FIG. 3. (Color online) The DSF $S(Q,\omega)$ at wave vectors $Q = 1.3$ and 1.7 Å^{-1} in films of liquid ^{4}He in 25-Å MPD gelsil at increasing filling, from filling 1 (F = 86% full) to filling 4 (F = 97%).

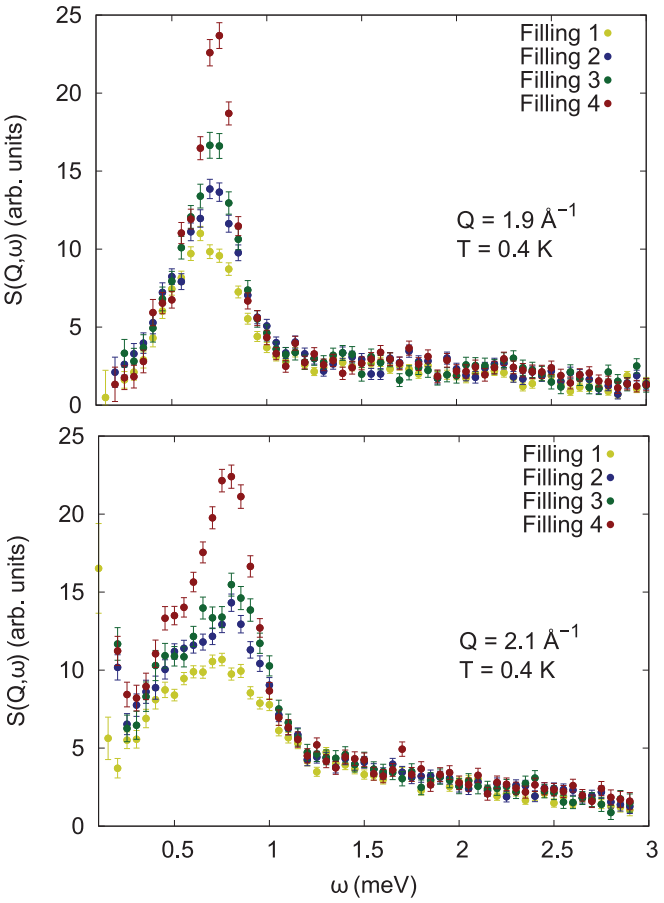

FIG. 4. (Color online) As Fig. 3 for $Q = 1.9$ and 2.1 Å^{-1}.

layer mode clearly co-exist in the first few liquid layers closest to the medium walls.

Figures 3 and 4 show the observed net $S(Q,\omega)$ versus ω at four specific Q values as a function of filling. At all Q, there is a broad contribution to $S(Q,\omega)$ that extends to high energy ω, which increases little with increasing filling. This is interpreted as inelastic scattering chiefly from the amorphous solid (inert) layers that are on the media walls at fillings F $\leqslant$ 70%. At $Q =$ 1.3 Å^{-1}, where the scattering is weak, there is a reasonably symmetric intensity which increases with increasing filling, which is interpreted as the P-R mode. At $Q = 2.1$ Å^{-1}, the asymmetric intensity is interpreted as the sum of the P-R mode, which peaks at $\omega = 0.75$ meV and a broad layer mode centered at $\omega \simeq 0.60$ meV.

Figure 5 shows the net $S(Q,\omega)$ at $Q = 1.9$ Å^{-1} at fillings F = 86% and F = 97% as a function of temperature. In Fig. 5, we see broad scattering extending to higher ω that is largely independent of temperature. In contrast, the intensity in the P-R mode decreases with increasing temperature and there is no identifiable P-R mode at temperatures $T \geqslant 1.9$ K. At $T = 2.0$ K, there is broad intensity peaked at $\omega \simeq 0.60$ meV that extends through the elastic region ($\omega = 0$) to negative energies. This is interpreted as scattering from the normal liquid, as observed in bulk liquid ^{4}He [29,30,32,54]. Since the layer mode (s) is also centered at $\omega \simeq 0.60$ meV, it is difficult to distinguish the layer mode from the normal liquid response at higher temperatures. It is thus difficult to determine the temperature dependence of the layer mode. Below we make model fits to the data.

B. Model fits to data

To identify the contributions to the total dynamic structure factors (DSF), $S(Q,\omega)$, we make fits of the model introduced in Sec. II to the data. The goal is particularly to determine the filling and temperature dependence of the P-R and layer modes.

1. Low temperature and filling dependence

At low temperature where the DSF of the normal component is negligible, the model $S(Q,\omega)$ in Eq. (1) reduces to Eq. (7). $S_{PR}(Q,\omega)$ and $S_L(Q,\omega)$ arising from P-R and layer modes, respectively, dominate $S(Q,\omega)$ in Eq. (7). $S_B(Q,\omega)$ is the observed DSF at a filling of 28% and represents scattering from the amorphous solid layers. $S_A(Q,\omega)$ is a small additional scattering from (a) the solid layers and (b) possible multiple scattering or multi-P-R scattering at higher fillings. $S_A(Q,\omega)$ is very small and contributes only at higher energy ($\omega \gtrsim 2$ meV).

Figure 6 shows examples of fits to data at $T = 0.4$ K and $Q = 1.30$ Å^{-1}. At $Q = 1.30$ Å^{-1}, there is no layer mode.

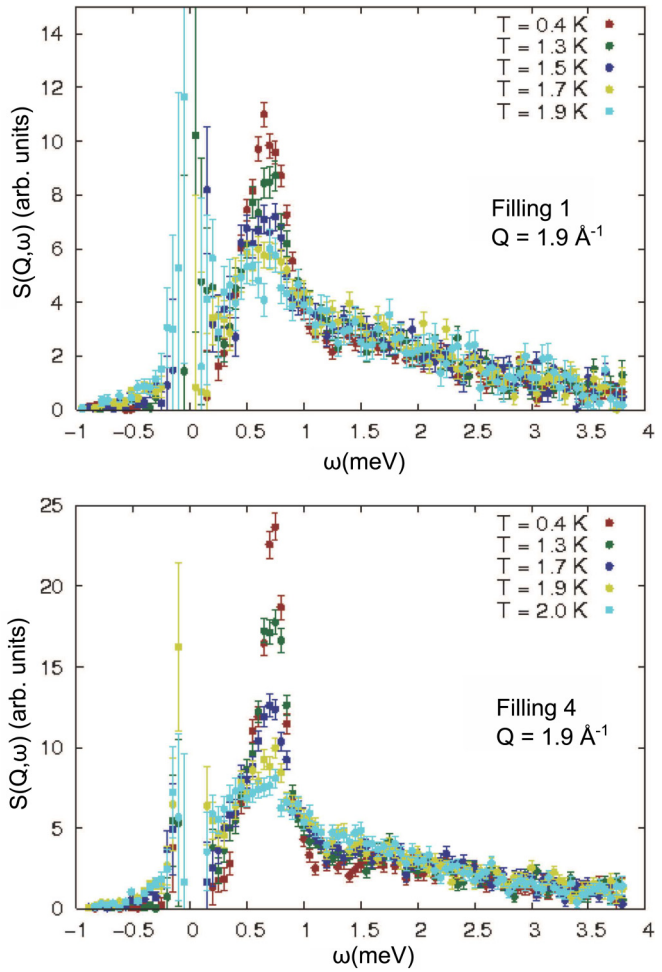

FIG. 5. (Color online) The temperature dependence of the DSF, $S(Q,\omega)$, at $Q = 1.9$ Å of liquid ^{4}He in gelsil at filling 1 (F = 86%) and filling 4 (F = 97%).

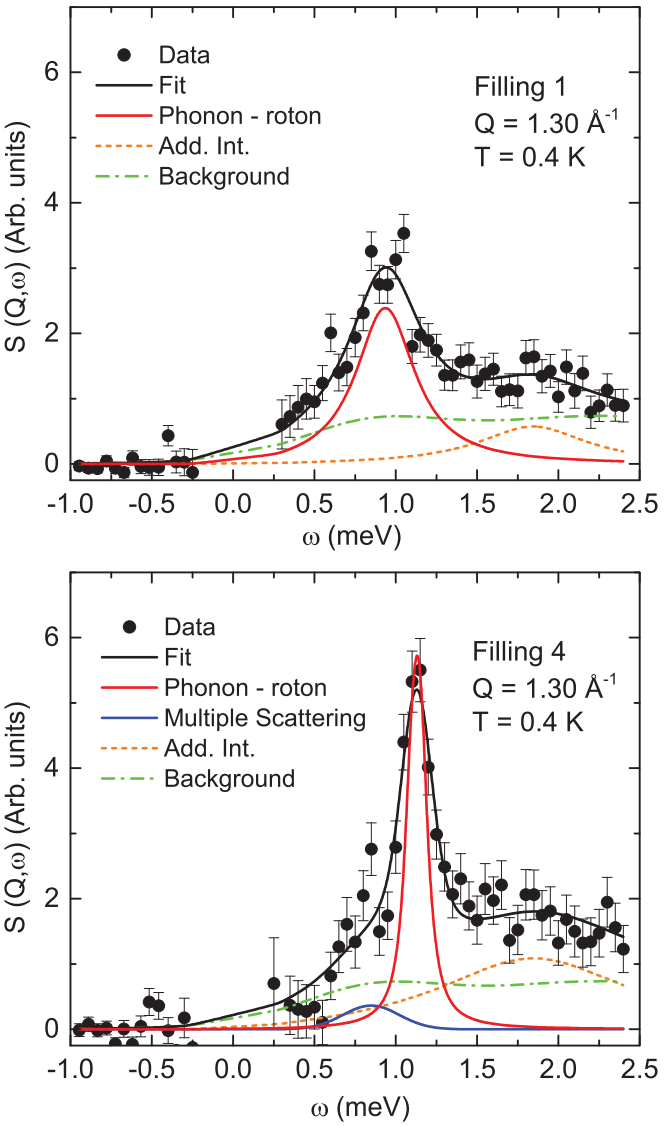

FIG. 6. (Color online) Observed $S(Q,\omega)$ (solid points) at $Q = 1.3$ Å^{-1} and $T = 0.4$ K with fits to data: upper frame is filling 1 (F = 86%) and the lower frame is filling 4 (F = 97%). The model $S(Q,\omega)$ is given by Eq. (1). It includes a background contribution (green long-short dashed line), denoted $S_B(Q,\omega)$ in Eq. (1), which is the observed intensity at filling F $\simeq$ 28% arising from the inert layers. The fitted components are the phonon-roton mode (red line) and some small additional intensity (Add. Int.) that contributes at higher energy needed to get a good fit at higher energy (brown short dashed line). They are denoted $S_{PR}(Q,\omega)$ and $S_A(Q,\omega)$ in Eq. (1), respectively. The total fitted $S(Q,\omega)$ (black line) is shown convoluted with the instrument resolution of 160 μeV. The P-R mode (red line) is not convoluted.

The remaining $S_{PR}(Q,\omega)$ is represented by the DHO function in Eq. (3) with Z_Q, Γ_Q, and ω_Q as fitting parameters. At filling 1, the P-R mode is broad. At filling 4 (F = 97%), the P-R mode has developed into a sharp, well-defined mode. There is also multiple scattering, an inelastic scattering from the intense roton at $Q = 1.9$ Å plus an elastic scattering from the gelsil, which modifies Q so that roton is observed at $Q = 1.3$ Å (as well as at other Q values). In Fig. 6, only the total $S(Q,\omega)$ given by the black solid line is convoluted with the IN6 instrument energy resolution function. A comparison of the convoluted total $S(Q,\omega)$ and the unconvoluted P-R mode shows that the observed P-R width at filling 4 arises chiefly from the instrument resolution.

Figure 7 shows similar fits of $S(Q,\omega)$ in Eq. (7) to data at $Q = 1.90$ Å^{-1} and $T = 0.4$ K. The intensity scale in Figs. 6 and 7 is the same. At $Q = 1.90$ Å^{-1}, there is a P-R and a layer mode with $S_L(Q,\omega)$ represented by Eq. (5). The intensity in the P-R mode increases significantly more rapidly with filling than does that of the layer mode. Again, only the total $S(Q,\omega)$ given by the black line is convoluted with IN6 instrument energy resolution function. To illustrate the filling dependence of the P-R and layer modes more directly, we show $S_{PR}(Q,\omega)$ and $S_L(Q,\omega)$ for four fillings in Fig. 8 with the background $S_B(Q,\omega)$ and $S_A(Q,\omega)$ components omitted for clarity.

There are several ways to characterize the intensity in $S(Q,\omega)$. The most reliable is simply the intensity integrated over ω, the static structure factor. These are given by Eqs. (9), (11), and (10) for each component of $S(Q,\omega)$. The $S(Q)$ were calculated analytically where possible and numerically otherwise. Figure 9 shows $S_{PR}(Q)$ versus filling at

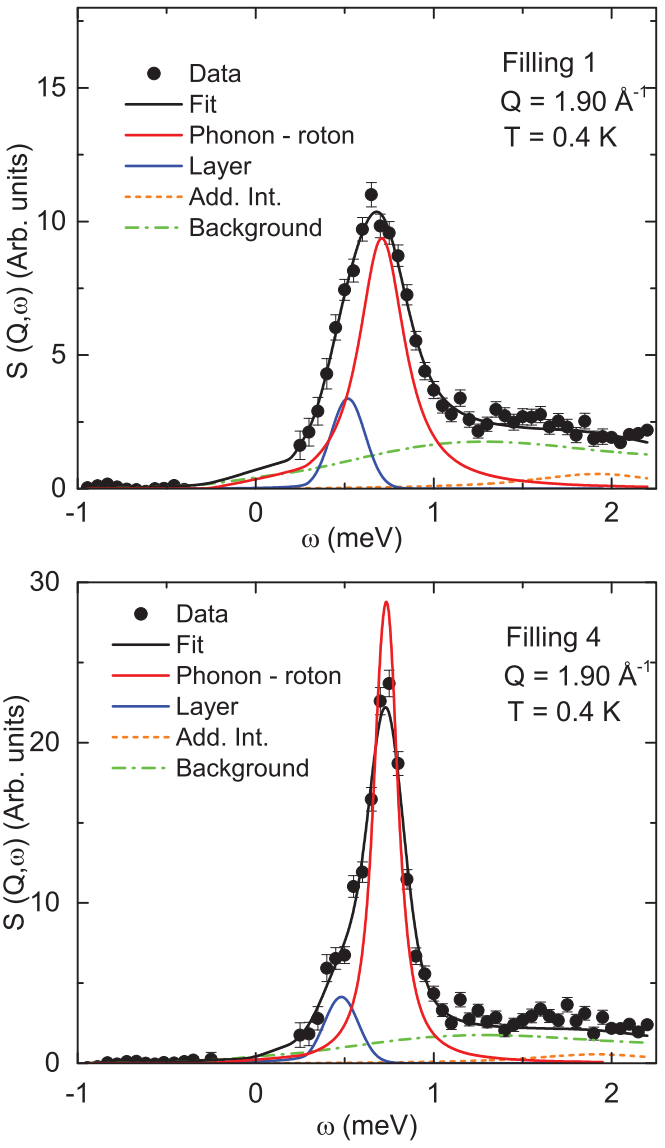

FIG. 7. (Color online) As Fig. 6 at $Q = 1.9$ Å^{-1} where a layer mode (solid blue line) as well as a P-R mode is observed. The intensity scale in Figs. 6 and 7 is the same.

$Q = 1.30$ Å^{-1} with a dotted line as a guide to the eye. Figure 10 shows $S_{PR}(Q)$ and $S_L(Q)$ versus filling at $Q = 1.90$ Å^{-1}. In Fig. 10, the dashed red line is the filling dependence of the intensity in the P-R mode observed by Plantevin *et al.* [26] with one overall magnitude adjustment. The same magnitude adjustment was used for the layer mode intensity (blue dashed line). Comparison of dashed blue line with the present blue points shows that the intensity in the layer mode relative to the P-R mode observed by Plantevin *et al.* is greater than observed in the present measurements. The reason for this is not clear.

2. *Temperature dependence*

In this section, we fit the model $S(Q,\omega)$ given by Eq. (1) to data as a function of temperature. A specific goal is to determine the temperature, T_{PR}, at which the P-R mode is no longer observed. In Eq. (1), $S_{PR}(Q,\omega)$, $S_L(Q)\omega$, and the

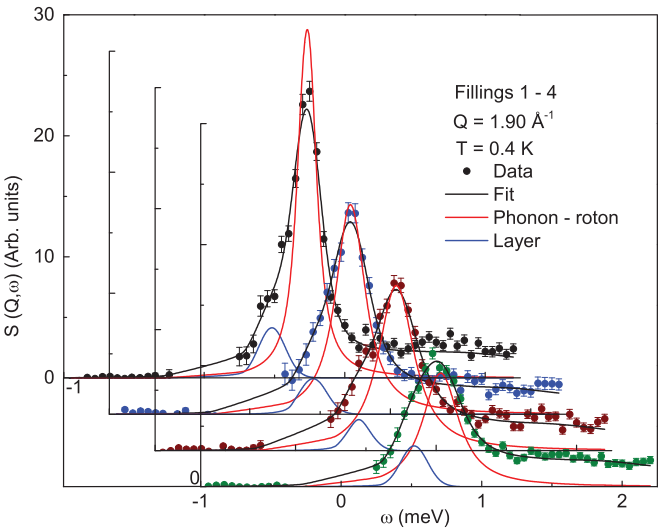

FIG. 8. (Color online) The observed $S(Q,\omega)$ (points) and the fitted phonon-roton (red line) and layer mode (blue line) components of $S(Q,\omega)$ vs filling. The increase in intensity in the P-R mode with filling can be readily seen. The background and additional intensity contributions to $S(Q,\omega)$ have been deleted for clarity.

normal liquid component, $S_N(Q,\omega)$ depend on temperature. In fits to data, the background and small additional intensity components were held independent of temperature at their $T = 0.4$ K values.

Figure 11 shows fits at $Q = 1.90$ Å^{-1} to data for filling 1 at three temperatures. Comparing the top frame of Fig. 11 ($T = 1.3$ K) with the top frame of Fig. 7 ($T = 0.4$ K), we see that the intensity in the P-R mode has already decreased significantly between $T = 0.4$ and 1.3 K. Also at $T = 1.3$ K, there is already significant intensity in the normal liquid component. At $T = 1.5$ K, the intensity in the P-R mode has decreased further and that in $S_N(Q,\omega)$ has increased. A small P-R mode is observed

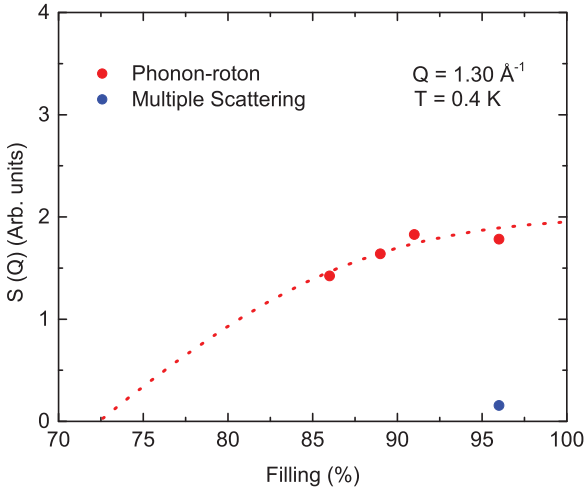

FIG. 9. (Color online) The integrated intensity, $S_{PR}(Q)$, in the phonon-roton (P-R) mode at $Q = 1.3$ Å^{-1} and $T = 0.4$ K vs filling (red points). The dotted line is a guide to the eye. In a previous measurement [26], the intensity in the P-R mode was first observed at filling F = 73%.

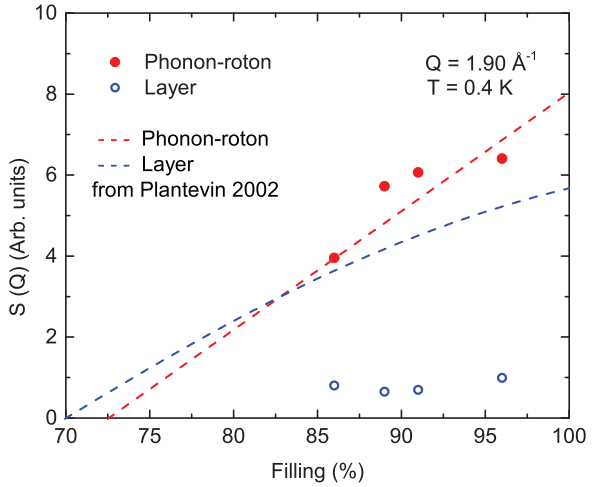

FIG. 10. (Color online) As Fig. 9 at $Q = 1.9$ Å^{-1}. The red points and blue points are the integrated intensity in the P-R and layer modes, respectively. The dashed red and dashed blue lines are the intensity in the P-R and layer modes, respectively, observed by Plantevin *et al.* [26], shown with one overall magnitude adjustment. The intensity in the layer mode observed here is smaller (relative to that of the roton) than observed by Plantevin *et al.*

at $T = 1.7$ K (not shown). At $T = 1.9$ K, there is no P-R mode and a best fit is obtained keeping only the normal component.

Figure 12 shows a similar fit to data for filling 4 as a function of temperature. The intensity in the P-R mode decreases with temperature with only modest mode broadening. At filling 4, a P-R mode is observed up to 1.9 K. At $T = 2.0$, 2.2, and 2.4 K, the observed intensity can be well reproduced including only $S_N(Q,\omega)$ (plus the temperature independent $[S_B(Q,\omega) + S_A(Q,\omega)]$) as shown in Fig. 12 at 2.2 K.

The static structure factors, $S_{\rm PR}(Q)$, $S_N(Q)$, and $S_L(Q)$ defined in Eqs. (9), (10), and (11), respectively, and calculated from the corresponding $S_{\rm PR}(Q,\omega)$, $S_N(Q,\omega)$, and $S_L(Q,\omega)$ are shown in Fig. 13 as a function of temperature. They represent the integrated intensity in each component as a function of temperature. In Fig. 13, we see that the integrated intensity in the P-R mode goes to zero at 1.75 ± 0.05 K at filling 1 and 1.90 ± 0.05 K at filling 4. Any intensity remaining in the layer mode at $T \geqslant 1.8$ K could not be separated from the much more intense $S_N(Q,\omega)$. It is satisfying that total $S(Q)$ is approximately independent of temperature as is observed in bulk liquid ^{4}He. The temperature dependence of the total $S(Q,\omega)$ in filling 4 is shown as a 3D color plot in Fig. 14.

C. Phase diagram

The superfluid phase of films of liquid ^{4}He in 25 Å MPD gelsil observed by Yamamoto *et al.* [4] is reproduced in Fig. 15. Shown is the superfluid phase as a function of filling and temperature. The threshold filling for the onset of superflow at $T = 0$ K in Fig. 15 is $n_0 = 20$ μmol/m^2. This value is somewhat less than the value $n_0 = 26$ μmol/m^2 observed [48] in several larger pore porous media. The gelsil used by Yamamoto *et al.* was fully filled at 33 μmol/m^2, shown as the dashed line in Fig. 15. The critical temperature

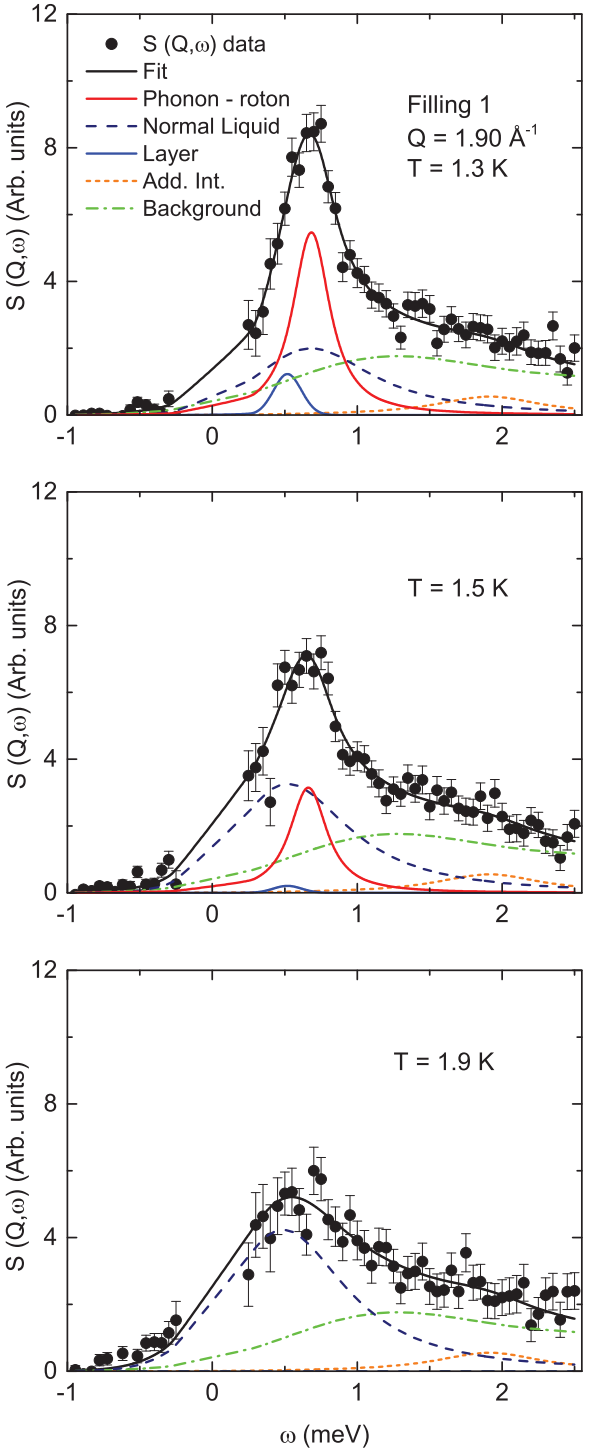

FIG. 11. (Color online) The temperature dependence of $S(Q,\omega)$ at $Q = 1.9$ Å^{-1} at filling 1 (F = 86%). Shown is $S(Q,\omega)$ at $T = 1.3$, 1.5, and 1.9 K. The solid dots are the data and the red and blue lines are the fitted phonon-roton and layer mode components, respectively. The normal liquid response is shown as a dashed blue line. The background and additional intensity components are held constant at their $T = 0.4$ K values independent of temperature. The intensity in the P-R mode decreases with temperature and vanishes by $T = 1.9$ K. At $T = 1.9$ K, only a normal liquid component, $S_N(Q,\omega)$ can be identified. At 1.9 K, there may be a layer mode but it cannot be separated from the $S_N(Q,\omega)$.

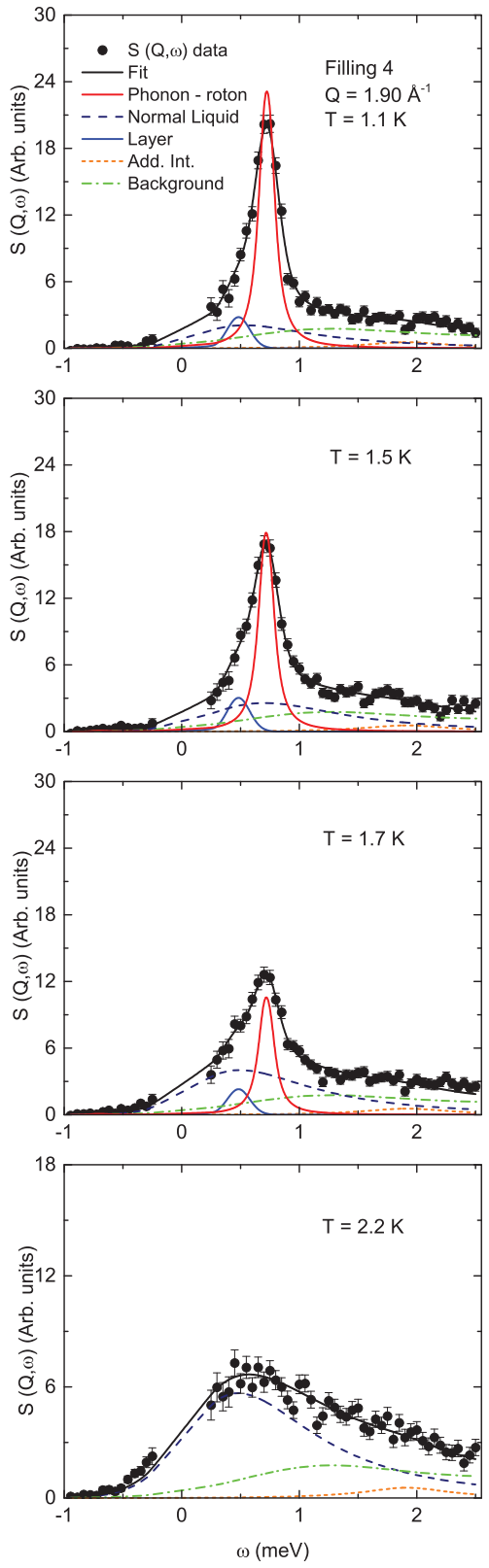

FIG. 12. (Color online) As Fig. 11 for filling 4 (F = 97%) at four temperatures.

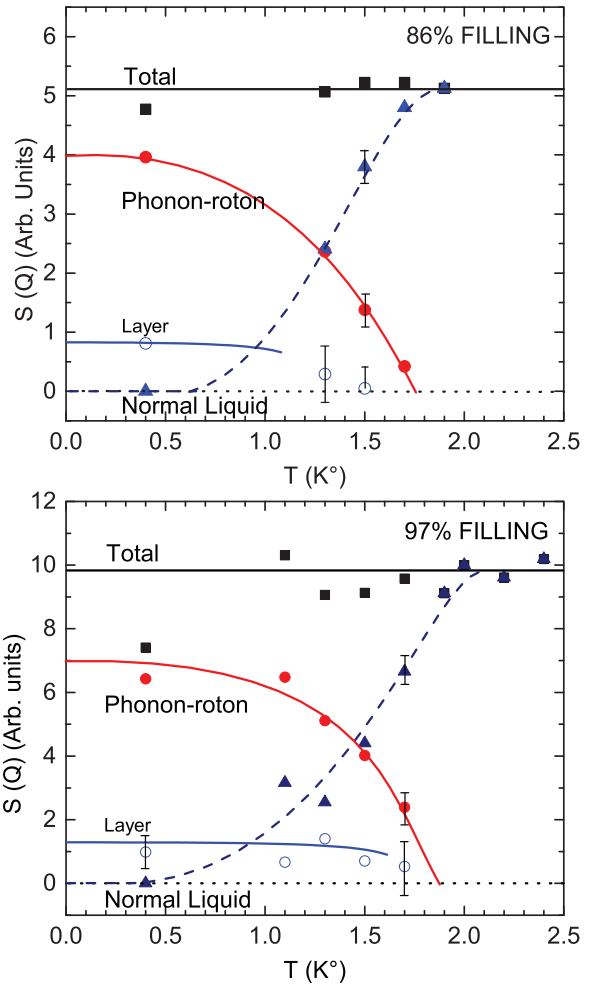

FIG. 13. (Color online) The integrated intensity $S(Q)$ at $Q = 1.90$ Å^{-1} in the P-R mode (red line), in the layer mode (blue line) and in the normal liquid response (dashed line) vs temperature for filling 1 (F = 86%) and filling 4 (F = 97%). The error bar shown on one P-R $S(Q)$ represents the error on all P-R $S(Q)$ and similarly for the other components. The total integrated intensity, $S(Q)$, (black squares), the sum of the three components, is approximately independent of temperature.

for superflow at full filling is $T_c = 1.45$ K. The temperatures, T_{PR}, at which the intensity in the P-R mode goes to zero is interpreted as the temperature T_{BEC} at which BEC goes to zero. These temperatures at fillings F = 86% and 97% are shown as T_{BEC} in Fig. 15. The temperature range $T_c < T < T_{BEC}$ is interpreted, as in fully filled media [4,8,16,20,26,28,55], as a region of localized BEC (LBEC) where there is BEC but no superflow. At low temperature (e.g., $T = 0.4$ K), P-R modes are first observed [26] at a filling of F = 73%. This filling is indicated by the dotted line in Fig. 15 and corresponds to $n = 25$ μmol/m^2. This filling is taken as the filling at which BEC first forms, i.e., the threshold filling for the onset of BEC. Superflow and BEC in films is discussed further in Sec. IV below.

To conclude, we note that it is difficult to compare absolute values of fillings from one sample to another and from one measurement to another. For example, we observed full filling at 28 μmol/m^2 (see Fig. 1) rather than the 33 μmol/m^2 reported by Yamamoto *et al.* The gelsil samples were from the same batch but were not exactly the same sample. They

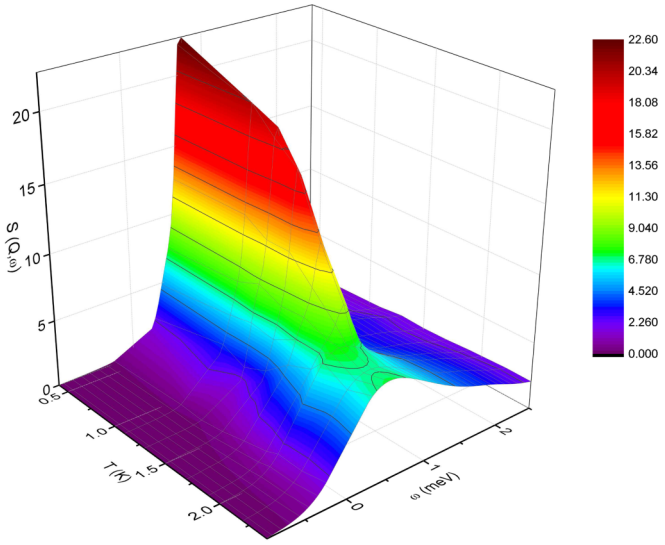

FIG. 14. (Color online) A 3D representation of the total fit $S(Q,\omega)$ vs temperature for filling 4.

were not filled under exactly the same conditions. Similarly, the threshold filling for superflow in several larger media [48] was not the same as that reported for gelsil [4]. For this reason, we have compared our results with those of Yamamoto *et al.* on the basis of percentage fillings, which we believe is more accurate.

IV. DISCUSSION

The chief purpose of the present paper is to determine whether there is a localized BEC (LBEC) phase in films of liquid ^{4}He. In fully filled porous media, there is a temperature range, $T_c < T < T_{\rm BEC}$, between the superfluid and fully normal phase where there is BEC but no superflow. This

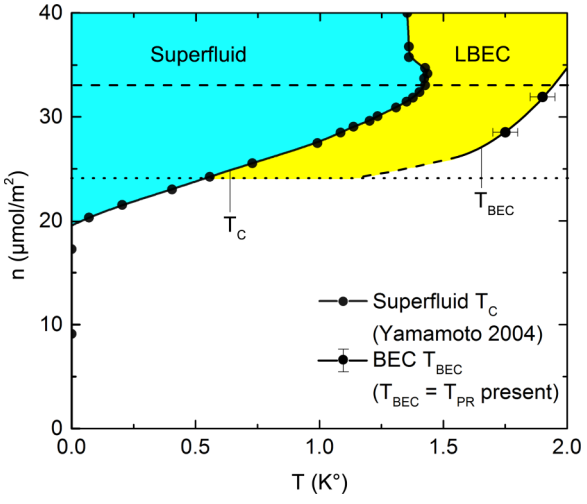

FIG. 15. (Color online) The phase diagram of films of liquid ^{4}He adsorbed in 25-Å MPD gelsil. Shown is the superfluid phase (blue) limited by T_c as observed by Yamamoto *et al.* [4] and the localized BEC (LBEC) region (yellow) limited at high temperature by $T_{\rm BEC} = T_{\rm PR}$, the temperature at which the intensity in the P-R mode goes to zero.

temperature range is interpreted as a phase in which the BEC is localized to islands separated by normal liquid in disorder. At temperatures $T_c < T < T_{\rm BEC}$, there is BEC and local superflow in the individual islands but no phase connection between the islands as needed for superflow across the sample. In fully filled pores, the existence of well-defined phonon-roton modes is taken as a signature of BEC. Our aim is to determine whether well define P-R modes in partially filled gelsil can also be observed above T_c.

As noted in the Introduction, a threshold coverage or threshold film thickness is needed in porous media before superfluidity is observed [48]. From Fig. 15, this coverage is $n_0 = 20$ μmol/m^2 in gelsil at low temperature [4]. At higher fillings, T_c increases approximately linearly with filling reaching $T_c = 1.4$ K at full filling [4]. Yamamoto *et al.* [4] observe full filling at 33 μmol/m^2 in present gelsils, which is indicated by the long dashed line in Fig. 15. There is similarly a critical coverage required before P-R modes are observed. Modes are first observed at a filling of 73% in the present gelsil (see Figs. 9 and 10), which corresponds to $n \simeq 24$ μmol/m^2 in the scale shown in Fig. 15 and is marked as a dotted line. Thus the onset fillings for P-R modes ($n \simeq 24$ μmol/m^2) and superfluidity at low temperature ($n \simeq 20$ μmol/m^2) are approximately the same. As filling is increased (from 73% to 100%), the phonon mode energies and intensities evolve in a smooth manner toward their full filling values (e.g., see Fig. 2). At full filling, the P-R mode energies are the same as in bulk liquid ^{4}He within precision.

From Figs. 13 to 15, we see that well-defined P-R modes are observed up to a temperature $T_{\rm PR} = 1.75$ and 1.9 K at fillings of 86% and 96%, respectively, as shown in Fig. 15. $T_{\rm PR}$ clearly lies well above T_c. Identifying $T_{\rm PR}$ with $T_{\rm BEC}$, we clearly have an LBEC "phase" in films near full filling as observed in fully filled gelsil [20,26] (as in a 3D liquid).

This result could be understood if BEC in 2D and 3D appear to be very similar in a small pore medium such as gelsil. BEC can be characterized by the one-body density matrix (OBDM), $n(r)$, which is the Fourier transform of the atomic momentum distribution, $n(k)$. In a 3D fluid when there is BEC, $n(r)$ has a tail at large r extending to $r = \infty$ of constant magnitude given by the condensate fraction, N_0/N. In 3D, the constant tail in $n(r)$ is denoted off-diagonal long-range order (ODLRO). The condensate state wave function also extends to $r = \infty$ with a well-defined phase, denoted phase coherence. In 2D, at low but finite temperature, the OBDM can have a long tail [56,57] but one that decays algebraically with r, denoted algebraic off-diagonal long-range order (AODLRO). Path integral Monte Carlo calculations [58] in bulk 2D liquid ^{4}He at $T = 0.675$ K show that this tail extends out to 100 Å or more. As a result, phase coherence over these length scales can be anticipated, i.e., effectively, BEC in 2D over length scales of 100 Å. In the LBEC phase, the picture is that BEC exists in islands of diameter 15–20 Å, which are large enough to support well-defined P-R modes at the wave lengths observed here. If this picture is correct, there may be little observable difference between the ODLRO in thick films of ^{4}He and fully filled pores in gelsil. In measurements of the condensate fraction [59], we have observed similar condensate fractions in films of helium and in bulk helium. In these measurements, the OBDM is observed out to lengths of 5–6 Å only. The ODBM is very

similar in 2D and 3D at the same density and temperature out to $r \simeq 6$ Å. Certainly, ^{4}He in gelsil does not show 1D behavior since BEC is not expected in 1D.

It is also possible that we are observing at least some fully filled gelsil in addition to films. To discuss this point, we note firstly that gelsil has a broad distribution of pore volumes (e.g., see Fig. 1 in Ref. [27]). At fillings of 86%, the smaller pore volumes, which fill first, can be expected to be full. However, since P-R modes are not observed at all until a filling of 73%, most of the smaller volumes do not contribute to the observed P-R modes. The observed P-R modes are supported predominantly by the liquid in the larger volumes, the last 27% of the gelsil to be filled.

Secondly, close to full filling (86% or greater), we may have capillary filling in the larger volumes. Capillary filling denotes filling in which those pores that have liquid in them are fully filled and further filling proceeds by fully filling more of the medium. In this case, we would be observing fully filled pore regions at partial fillings. The adsorption isotherm in Fig. 1 does not indicate capillary filling behavior. Capillary filling is indicated by an upturn in the isotherm. An upturn is seen in Vycor, which has pores. The apparent lack of capillary filling is probably because gelsil consists of a distribution of volumes not pores. Thirdly, the larger volumes in gelsil are interconnected. Interconnected pores have been proposed to explain why superfluid critical exponent in Vycor has the bulk 3D value [2,10] and why a dilute gas of ^{4}He in Vycor shows 3D behavior [45,60]. We do not expect the interconnected nature to affect the P-R modes directly, only enable films to exist. In summary, while at least some fully filled regions are being observed, we believe that P-R modes observed originate predominately from liquid that has a surface in the larger pore volumes.

The integrated intensity in the layer mode (or modes) shown here is less than that determined in the same gelsil by Plantevin *et al.* [26] (see Fig. 10 for a comparison). The energy and width of the layer mode intensity agrees well. This difference in intensity probably arises from a difference in the fitting procedure. The broad layer mode overlaps with the more intense P-R mode (see Figs. 7 and 8) making it difficult to extract the layer mode in a unique fashion. There could also be a difference in surface preparation (cleaning). In a recent measurement in FSM, Prisk *et al.* [22] observe a layer mode intensity similar to that observed by Plantevin *et al.* [26].

For similar fitting reasons we were not able to determine the temperature dependence of the layer mode at higher temperature ($T > 1.5$ K) (see Fig. 13). The broad intensity of the layer mode centered at $\omega = 0.6$ meV lies in the same energy range as the maximum of the even broader normal liquid intensity at higher temperature. For this reason, the layer mode cannot be separated from the normal liquid response at higher temperature. In contrast, at higher pressure (e.g., 34 bar), we were able to determine the temperature dependence of the layer mode. At higher pressure, the response of normal liquid ^{4}He peaks near $\omega = 0$ as it does in classical liquids. Under pressure, the normal liquid responds much like a classical liquid. In this case, the layer mode at $\omega = 0.6$ meV can be distinguished from the normal liquid intensity. The layer mode continues to exist at temperatures above $T_{\rm PR}$ where the roton has vanished. It continues to exist in the fully normal phase so that the existence of the layer mode is apparently not related to BEC.

V. CONCLUSION

We have measured the dynamic structure factor, $S(Q,\omega)$, of liquid ^{4}He films in 25-Å diameter gelsil as a function of film thickness and temperature. At low temperature, where there is superfluidity and apparently BEC, $S(Q,\omega)$ contains the P-R mode and a layer mode. As temperature is increased, the P-R mode gives way to broad normal liquid response. However, well defined P-R modes continue to be observed at temperatures above the superfluid onset temperature, T_c. This is interpreted as BEC remaining at temperatures above T_c and a localized BEC "phase" lying between the superfluid and normal phase similar to the pseudogap phase in the cuprate superconductors.

ACKNOWLEDGMENTS

It is a pleasure to acknowledge the support of the Institut Laue Langevin and O. Losserand and X. Tonon at ILL for valuable assistance with the experiments. This work was supported by the DOE, Office of Basic Energy Sciences under contract No. ER46680.

APPENDIX: MODELS OF $S(Q,\omega)$

In bulk liquid ^{4}He, two models are commonly used to describe the temperature dependence of $S(Q,\omega)$, denoted the Woods-Svensson (WS) and Simple-Subtraction (SS) models. In the WS model, $S(Q,\omega)$ is expressed as the sum of a P-R mode (and a multi-P-R component), $[S_{\rm PR}(Q,\omega) + S_M(Q,\omega)]$, which is proportional to the superfluid fraction, $\rho_S(T)/\rho$, and a normal liquid component, $S_N(Q,\omega)$, proportional to $[1 - \rho_S(T)/\rho]$: $S(Q,\omega) = \rho_S(T)/\rho[S_{\rm PR}(Q,\omega) + S_M(Q,\omega)] + (1 - \rho_S(T)/\rho)S_N(Q,\omega)$. $S_M(Q,\omega)$ is small compared to $S_{\rm PR}(Q,\omega)$. In this model, the contribution of the P-R mode to $S(Q,\omega)$ goes to zero at T_λ. The WS model describes the temperature dependence of $S(Q,\omega)$ quite well for wave vectors $Q \geqslant 0.8$ Å. At low Q, there is a sound mode that survives into the normal phase, i.e., there is sound propagation in normal liquid ^{4}He as in all liquids.

In the SS model, a background and multi-P-R mode contribution is first identified at low temperature. This is simply subtracted from the data. A single $S_{\rm PR}(Q,\omega)$ is then fitted to the remaining data at all temperatures. In the SS model, the $S_{\rm PR}(Q,\omega)$ broadens into a flat, featureless intensity at T_λ but intensity remains above T_λ. To understand this, we note that the static structure factor $S(Q)$ of liquid ^{4}He is roughly independent of temperature ($\pm 5\%$). Since, after subtraction of a constant background, the remaining integrated intensity over $S_{\rm PR}(Q,\omega)$ is proportional to $S(Q)$, the integrated intensity in $S_{\rm PR}(Q,\omega)$ must remain roughly independent of temperature and cannot go to zero at T_λ. The drawbacks of these models is that in the WS model the intensity in the P-R mode must go to zero at T_λ whereas in the SS model the intensity must remain in the P-R mode above T_λ. In either model, there is no well-defined P-R mode at T_λ and above T_λ.

In a recent paper [21] on modes in liquid ^{4}He under pressure in MCM-41, we used a model consisting of a P-R mode, $S_{PR}(Q,\omega)$, a layer mode, $S_L(Q,\omega)$, and a normal liquid component $S_N(Q,\omega)$. $S_{PR}(Q,\omega)$ and $S_L(Q,\omega)$ were determined from fits to data at low temperature. $S_N(Q,\omega)$ was determined from fits to data at the highest temperature. To represent the temperature dependence, $S_{PR}(Q,\omega)$ was multiplied by a weight f_{PR} and $S_N(Q,\omega)$ was multiplied by (1 - f_{PR}). The $f_{PR}(T)$ was determined by fits to data as a function of T with fine tuning of $S_{PR}(Q,\omega)$. A similar representation of $S_L(Q,\omega)$ was made. In this model, the $f_{PR}(T)$ can take any value at any intermediate temperature. However, a temperature independent $S(Q)$ has been built into the model. The intensity f_{PR} in the P-R mode was found [21] to go to zero at a low temperature 1.45 K at 34 bar.

In the present model, the three parameters in $S_{PR}(Q,\omega)$, $S_L(Q,\omega)$, and $S_N(Q,\omega)$ were determined independently at each temperature and can take any value. There is no predetermined dependence of the parameters on temperature. The integrated intensity $S(Q)$ in each component can take any value and it is satisfying that the total $S(Q)$ of all three is approximately independent of temperature as is observed in the bulk liquid.

The Z_Q of the DHO or Gaussian functions could be used to identify the intensity. Z_Q is a reliable indicator of intensity for a DHO provided the DHO is narrow (small Γ_Q) and the energy ω_Q is reasonably large. It is not reliable for the normal liquid component where Γ_Q is large and ω_Q is small. In this case, since the product $\omega_Q Z_Q$ appears in the numerator of the DHO, Z_Q gets very large when ω_Q gets small. At higher temperature, ω_Q goes to zero and Z_Q ceases to represent the intensity. To represent the integrated intensity, we use the static structure factors given by Eqs. (9) to (11). These $S(Q)$ were calculated from the corresponding fitted $S(Q,\omega)$ and represent the intensity accurately for any shape of $S(Q,\omega)$.

[1] D. F. Brewer, in *The Physics of Liquid and Solid Helium, Part II*, edited by K. H. Benneman and J. B. Ketterson (Wiley, New York, 1978), p. 573.
[2] J. D. Reppy, J. Low Temp. Phys. **87**, 205 (1992).
[3] M. H. W. Chan, M. Mulders, and J. D. Reppy, Phys. Today **49**(8), 30 (1996).
[4] K. Yamamoto, H. Nakashima, Y. Shibayama, and K. Shirahama, Phys. Rev. Lett. **93**, 075302 (2004).
[5] N. Wada, J. Taniguchi, H. Ikegami, S. Inagaki, and Y. Fukushima, Phys. Rev. Lett. **86**, 4322 (2001).
[6] N. Wada, Y. Minato, T. Matsushita, and M. Hieda, J. Phys. Soc. Jpn. **77**, 111012 (2008).
[7] N. Wada, Y. Minato, T. Matsushita, and M. Hieda, J. Low Temp. Phys. **162**, 549 (2011).
[8] J. Taniguchi, Y. Aoki, and M. Suzuki, Phys. Rev. B **82**, 104509 (2010).
[9] J. Taniguchi, R. Fujii, and M. Suzuki, Phys. Rev. B **84**, 134511 (2011).
[10] M. H. W. Chan, K. I. Blum, S. Q. Murphy, G. K. S. Wong, and J. D. Reppy, Phys. Rev. Lett. **61**, 1950 (1988).
[11] G. M. Zassenhaus and J. D. Reppy, Phys. Rev. Lett. **83**, 4800 (1999).
[12] F. Albergamo, H. R. Glyde, D. R. Daughton, N. Mulders, J. Bossy, and H. Schober, Phys. Rev. B **69**, 014514 (2004).
[13] S. Miyamoto and Y. Takano, Czech. J. Phys. **46**, 139 (1996).
[14] K. Huang and H. F. Meng, Phys. Rev. B **48**, 6687 (1993).
[15] C. W. Kiewiet, H. E. Hall, and J. D. Reppy, Phys. Rev. Lett. **35**, 1286 (1975).
[16] H. R. Glyde, O. Plantevin, B. Fak, G. Coddens, P. S. Danielson, and H. Schober, Phys. Rev. Lett. **84**, 2646 (2000).
[17] B. Fåk, O. Plantevin, H. R. Glyde, and N. Mulders, Phys. Rev. Lett. **85**, 3886 (2000).
[18] O. Plantevin, B. Fåk, H. R. Glyde, N. Mulders, J. Bossy, G. Coddens, and H. Schober, Phys. Rev. B **63**, 224508 (2001).
[19] J. V. Pearce, S. O. Diallo, H. R. Glyde, R. T. Azuah, T. Arnold, and J. Z. Larese, J. Phys.: Condens. Matter **16**, 4391 (2004).
[20] F. Albergamo, J. Bossy, J. V. Pearce, H. Schober, and H. R. Glyde, Phys. Rev. B **76**, 064503 (2007).
[21] J. Bossy, J. Ollivier, H. Schober, and H. R. Glyde, Europhys. Lett. **98**, 56008 (2012).
[22] T. R. Prisk, N. C. Das, S. O. Diallo, G. Ehlers, A. A. Podlesnyak, N. Wada, S. Inagaki, and P. E. Sokol, Phys. Rev. B **88**, 014521 (2013).
[23] R. M. Dimeo, P. E. Sokol, C. R. Anderson, W. G. Stirling, K. H. Andersen, and M. A. Adams, Phys. Rev. Lett. **81**, 5860 (1998).
[24] C. R. Anderson, W. G. Stirling, K. H. Andersen, P. E. Sokol, and R. M. Dimeo, Physica B **276-278**, 820 (2000).
[25] C. R. Anderson, K. H. Andersen, W. G. Stirling, P. E. Sokol, and R. M. Dimeo, Phys. Rev. B **65**, 174509 (2002).
[26] O. Plantevin, H. R. Glyde, B. Fåk, J. Bossy, F. Albergamo, N. Mulders, and H. Schober, Phys. Rev. B **65**, 224505 (2002).
[27] J. Bossy, J. V. Pearce, H. Schober, and H. R. Glyde, Phys. Rev. Lett. **101**, 025301 (2008).
[28] K. Yamamoto, Y. Shibayama, and K. Shirahama, Phys. Rev. Lett. **100**, 195301 (2008).
[29] A. D. B. Woods and E. C. Svensson, Phys. Rev. Lett. **41**, 974 (1978).
[30] E. F. Talbot, H. R. Glyde, W. G. Stirling, and E. C. Svensson, Phys. Rev. B **38**, 11229 (1988).
[31] K. H. Andersen, W. G. Stirling, R. Scherm, A. Stunault, B. Fåk, A. Godfrin, and A. J. Dianoux, J. Phys.: Condens. Matter **6**, 821 (1994).
[32] K. H. Andersen and W. G. Stirling, J. Phys.: Condens. Matter **6**, 5805 (1994).
[33] G. Zsigmond, F. Mezei, and M. T. F. Telling, Physica B **388**, 43 (2007).
[34] P. Nozières and D. Pines, *Theory of Quantum Liquids* (Addison-Wesley, Redwood City, CA, 1990), Vol. II.
[35] N. N. Bogoliubov, J. Phys. (Moscow) **11**, 23 (1947).
[36] J. Gavoret and P. Nozières, Ann. Phys. **28**, 349 (1964).
[37] P. C. Hohenberg and P. C. Martin, Ann. Phys. **34**, 291 (1965).
[38] H. R. Glyde and A. Griffin, Phys. Rev. Lett. **65**, 1454 (1990).
[39] A. Griffin, *Excitations in a Bose Condensed Liquid* (Cambridge University Press, Cambridge, 1993).
[40] J. Bossy, J. V. Pearce, H. Schober, and H. R. Glyde, Phys. Rev. B **78**, 224507 (2008).

[41] I. Rudnick and J. Fraser, J. Low Temp. Phys. **3**, 225 (1970).
[42] M. Chester and L. C. Yang, Phys. Rev. Lett. **31**, 1377 (1973).
[43] J. E. Berthold, D. J. Bishop, and J. D. Reppy, Phys. Rev. Lett. **39**, 348 (1977).
[44] D. J. Bishop and J. D. Reppy, Phys. Rev. Lett. **40**, 1727 (1978).
[45] B. C. Crooker, B. Hebral, E. N. Smith, Y. Takano, and J. D. Reppy, Phys. Rev. Lett. **51**, 666 (1983).
[46] P. A. Crowell, F. W. Van Keuls, and J. D. Reppy, Phys. Rev. B **55**, 12620 (1997).
[47] A. Corwin, J. He, G. Zassenhaus, and J. Reppy, J. Low Temp. Phys. **121**, 525 (2000).
[48] G. A. Csáthy, J. D. Reppy, and M. H. W. Chan, Phys. Rev. Lett. **91**, 235301 (2003).
[49] K. Shirahama, K. Yamamoto, and Y. Shibayama, Low Temp. Phys. **34**, 273 (2008).
[50] K. Yamamoto, Y. Shibayama, and K. Shirahama, J. Phys. Soc. Jpn. **77**, 013601 (2008).
[51] E. P. Barrett, L. G. Joyner, and P. P. Halenda, J. Am. Chem. Soc. **73**, 373 (1951).
[52] H. R. Glyde, *Excitations in Liquid and Solid Helium* (Oxford University Press, Oxford, 1994).
[53] B. Fåk, L. P. Regnault, and J. Bossy, J. Low Temp. Phys. **89**, 345 (1992).
[54] W. G. Stirling and H. R. Glyde, Phys. Rev. B **41**, 4224 (1990).
[55] F. Albergamo, J. Bossy, P. Averbuch, H. Schober, and H. R. Glyde, Phys. Rev. Lett. **92**, 235301 (2004).
[56] D. M. Ceperley and E. L. Pollock, Phys. Rev. B **39**, 2084 (1989).
[57] D. M. Ceperley, Rev. Mod. Phys. **67**, 279 (1995).
[58] M. Boninsegni, N. V. Prokof'ev, and B. V. Svistunov, Phys. Rev. E **74**, 036701 (2006).
[59] S. O. Diallo, J. V. Pearce, R. T. Azuah, J. W. Taylor, and H. R. Glyde, Phys. Rev. B **78**, 024512 (2008).
[60] J. D. Reppy, B. C. Crooker, B. Hebral, A. D. Corwin, J. He, and G. M. Zassenhaus, Phys. Rev. Lett. **84**, 2060 (2000).